Monthly Notices
of the
ROYAL ASTRONOMICAL SOCIETY

MNRAS **465,** 4044–4056 (2017)
Advance Access publication 2016 November 22

doi:10.1093/mnras/stw2985

Dust masses for SN 1980K, SN1993J and Cassiopeia A from red–blue emission line asymmetries

Antonia Bevan,[1]★ M. J. Barlow[1] and D. Milisavljevic[2]

[1]*Department of Physics and Astronomy, University College London, Gower Street, London WC1E 6BT, UK*
[2]*Harvard–Smithsonian Center for Astrophysics, 60 Garden Street, Cambridge, MA 02138, USA*

Accepted 2016 November 15. Received 2016 November 14; in original form 2016 September 13

ABSTRACT

We present Monte Carlo line transfer models that investigate the effects of dust on the very late time emission line spectra of the core-collapse supernovae SN 1980K and SN 1993J and the young core collapse supernova remnant Cassiopeia A. Their blueshifted emission peaks, resulting from the removal by dust of redshifted photons emitted from the far sides of the remnants, and the presence of extended red emission wings are used to constrain dust compositions and radii and to determine the masses of dust in the remnants. We estimate dust masses of between 0.08 and 0.15 $M_\odot$ for SN 1993J at year 16, 0.12 and 0.30 $M_\odot$ for SN 1980K at year 30 and ∼1.1 $M_\odot$ for Cas A at year ∼330. Our models for the strong oxygen forbidden lines of Cas A require the overall modelled profiles to be shifted to the red by between 700 and 1000 km s^{-1}, consistent with previous estimates for the shift of the dynamical centroid of this remnant.

Key words: radiative transfer – supernovae: general – supernovae: individual: SN 1980K, SN 1993J, Cas A – ISM: supernova remnants.

1 INTRODUCTION

The large quantities of dust observed in some high-redshift galaxies may have been produced by supernovae (SNe) from massive stars, although a high dust formation efficiency of 0.1–1.0 $M_\odot$ per SN appears to be required (Morgan & Edmunds 2003; Dwek, Galliano & Jones 2007). Quantitative determinations of the masses of dust formed in the ejecta of core-collapse supernovae (CCSNe) have normally relied on modelling their thermal infrared (IR) dust emission spectra, (Dwek et al. 1983; Wooden et al. 1993; Sugerman et al. 2006; Gall, Hjorth & Andersen 2011; Gomez et al. 2012; Indebetouw et al. 2014; Matsuura et al. 2015, and other workers). However, even with the enhanced sensitivities of modern thermal IR instruments, it has been difficult to detect extragalactic SNe at wavelengths longwards of 8 μm more than 3 yr after outburst.

An alternative method to determine dust masses in CCSN ejecta was proposed by Lucy et al. (1989) and applied by them to analyse the optical spectra of SN 1987A, whose Hα and [O I] line profiles from 2 yr after outburst onwards showed pronounced red–blue asymmetries, with their peak line emission shifted bluewards from line centre. This was interpreted and modelled as due to redshifted photons emitted from the far side of the ejecta suffering more absorption by newly formed dust grains than blueshifted photons emitted from the near side. They noted an additional effect, whereby energy lost by dust-scattered photons can lead to a red emission wing extending to higher velocities than the largest velocity seen at the blue edge of the line profile.

In order to exploit the above phenomena to derive SN dust masses from their observed late-time emission line profiles, Bevan & Barlow (2016) have developed a Monte Carlo line transfer code, DAMOCLES, that models line photons subjected to scattering and absorption by dust in expanding ejecta. The emitting material can have arbitrary velocity and density distributions and the code can handle a wide range of grain species and grain size distributions. Bevan & Barlow (2016) used DAMOCLES to model the asymmetric Hα and [O I] emission line profiles of SN 1987A between days 714 and 3604, finding that the mass of dust in the ejecta had increased from $\leq 1.5 \times 10^{-3}$ $M_\odot$ on day 714 to ≥ 0.1 $M_\odot$ on day 3604. They also found that the presence of extended red emission wings in the observed line profiles at these epochs placed lower limits on the grain albedos, requiring grain radii ≥ 0.6 μm.

Blueshifted line emission can be a common and long-lasting feature of the optical spectra of some CCSNe, with emission lines of oxygen and hydrogen often exhibiting red–blue asymmetries and significant substructure at both early times (e.g. SN 2006jc, Smith et al. 2008; SN 2005ip, SN 2006jd, Stritzinger et al. 2012 and SN 2010jl, Smith et al. 2012; Gall et al. 2014) and at late times (e.g. Milisavljevic et al. 2012). If these lines can be modelled, then it may be possible to determine the masses of dust in SN ejecta and supernova remnants (SNRs). This is particularly useful at late-time epochs ($\gtrsim$5 yr) where CCSNe are not currently accessible at mid-IR and longer wavelengths.

★ E-mail: antonia.bevan.12@ucl.ac.uk

Of a sample of 10 extragalactic CCSNe with ages of up to 50 yr that were detected via optical spectroscopy by Milisavljevic et al. (2012), more than 50 per cent exhibited blueshifted emission line profiles. A range of energy sources can potentially illuminate such late epoch ejecta, e.g. irradiation by photons from a nearby OB cluster; or from the interaction between the forward shock and surrounding circumstellar material, ionization of the ejecta by a reverse shock or photoionization by a central pulsar or magnetar (Chevalier & Fransson 1992, 1994).

In this paper, we present DAMOCLES models and dust mass estimates based on the late-time emission line spectra of two of the extragalactic SNe observed by Milisavljevic et al. (2012) with good signal to noise, SN 1980K and SN 1993J. In addition, we model the asymmetric line profiles seen in the optical spectrum of the ∼330-yr-old Galactic SNR Cassiopeia A, whose integrated spectrum was shown by Milisavljevic et al. (2012), and present dust mass estimates for this remnant. If placed at a distance of 1 Mpc, this 5 arcmin diameter SNR would have an angular diameter of just ∼1 arcsec, so its integrated spectrum may provide a parallel to the spectra of extragalactic SNRs of a similar age. In Section 2, we describe the observational data for SN 1980K and SN 1993J and discuss the process of fitting their spectra. Section 3 presents models for the Hα and [O I] profiles of SN 1980K processed by smooth distributions and clumped distributions of dust, while in Sections 4 and 5 we do the same for the oxygen line profiles of SN 1993J and Cas A, respectively. We summarize our conclusions in Section 6.

2 SN 1980K AND SN 1993J

SN 1980K is located in NGC 6946, at a distance of approximately 5.9 Mpc (Karachentsev, Sharina & Huchtmeier 2000). It was discovered by P. Wild on 1980 October 28 and had reached a peak brightness of $V = 11.4$ mag by November that year (Buta 1982). The detection of a broad Hα line in early spectra and a linearly decaying light curve after peak brightness resulted in its classification as a Type IIL SNe (Barbon, Ciatti & Rosino 1982). SN 1980K continued to decline steadily in the optical although it was still detected almost 7 yr after maximum light by narrow passband imaging by Fesen & Becker (1988), whose follow-up low dispersion observations found that the spectra exhibited broad Hα and [O I] $\lambda\lambda$6300,6363 emission, with other weaker optical lines also present.

Spectroscopic and photometric observations of SN 1980K have revealed a very slow monotonic fading over a period of ∼20 yr. This unusually slow rate of decline suggested that the observations may in fact be a product of light echoes scattering off and heating circumstellar material. This was first suggested by Chevalier (1986) based on observations during the first year after outburst. From further modelling and analyses of late-time observations, Sugerman et al. (2012) concluded that light echoes were indeed present and that the evolution of the observations could be explained by scattered and thermal echoes off a thin circumstellar shell of dust of mass $\lesssim$0.02 $M_\odot$ approximately 14–15 light years from the progenitor. Of particular relevance was their discussion of the origin of the broad, high-velocity Hα and [O I] $\lambda\lambda$6300,6363 lines which were not present in early spectra taken during the first 2 yr. They concluded that the shape of these lines could not be a product of a light echo since the high velocities seen in the late-time spectra were not present in early spectra.

In 1981, the emergence of a near-IR flux excess had provided the first indications of dust in the ejecta of SN 1980K (Dwek et al. 1983). However, it could not be confirmed whether this excess IR flux was the result of newly formed dust condensing in the ejecta or came from pre-existing grains located in a circumstellar shell illuminated by radiation from the outburst. In addition to the detection of the signature emission from hot dust grains in the near-IR, highly blueshifted line profiles in the optical spectra of SN 1980K have been observed for a number of years after (Fesen & Becker 1990; Fesen & Matonick 1994; Fesen, Hurford & Matonick 1995; Fesen et al. 1999). The presence of dust in its ejecta was postulated by Milisavljevic et al. (2012) based on the observed blueshifting of the optical line profiles, still present even in very late-time spectra (30 yr). It is these late blueshifted line profiles of SN 1980K at 30 yr that we have modelled and present here. An explosion date of 1980 October 2 (Montes et al. 1998) was adopted for all models.

SN 1993J is a very well-observed SN and is only surpassed by SN 1987A in regard to the quality and frequency of its observations. It is located in the nearby M 81 galaxy, 3.6 Mpc away (Freedman et al. 1994), and was discovered on 1993 March 28 (Ripero et al. 1993). It reached a maximum brightness of $V = 10.8$ mag making it the brightest SN in the Northern hemisphere since SN 1954A. Early spectra showed typical Type II features including broad Hα emission. However, its evolution was atypical and the appearance of He lines in later spectra resulted in its classification as Type IIb. The similarities to Type Ib and Type Ic SNe were noted however and this SN has been important for understanding the relationship between the Type I and Type II CCSN categories (Filippenko, Matheson & Ho 1993; Garnavich & Ann 1993). Extensive reviews of SN 1993J are given by Wheeler & Filippenko (1996), who cover the early evolution of the object, and by Matheson et al. (2000a,b), who discuss the later evolution of the optical spectra.

The relatively isolated and nearby position of SN 1993J led to regular monitoring at X-ray, radio and optical wavelengths. We were particularly interested in late-time optical spectra obtained at 16 years post-outburst and the presence, or otherwise, of dust in the ejecta as postulated by Fransson et al. (2005) and Milisavljevic et al. (2012). An explosion date of 1993 March 27 (Baron et al. 1993) is adopted for all models.

2.1 Fitting the late-time optical spectra of SN 1980K and SN 1993J

Late-time spectra of both SN 1980K and SN 1993J were published by Milisavljevic et al. (2012) and we present them here in Fig. 1.

The spectra of SN 1980K were obtained on 2010 October 9 using the 2.4 m Hiltner telescope at the MDM observatory. The Mark III Spectrograph was used with an SITe 1024 × 1024 CCD detector and a 1.2 arcsec × 4.5 arcmin slit. Exposures were 2 × 3000 s and spectra spanned the wavelength range 4600–8000 Å with a spectral resolution of 7 Å. The spectrum presented in fig. 1 is of SN 1980K at approximately 30 yr after outburst. Significant blueshifting can be seen in virtually all lines, but especially in the Hα and [O I] λ6300,6363 lines which exhibit a pronounced flux bias towards the blue and a strongly blueshifted peak (see Fig. 1). Narrow nebular lines of Hα and [O III] provide useful rest velocity reference points and the small recession velocity of 40 km s^{-1} of NGC 6946 has been corrected for.

The optical spectrum of SN 1993J was obtained on 2009 December 9 with the 6.5m MMT at Mt Hopkins in Arizona using the HECTOSPEC optical fibre-fed spectrograph. Spectra from the 1.5 arcsec diameter fibres covered the wavelength range of 3700–9200 Å with a full-width at half-maximum (FWHM) resolution of 5 Å. The total exposure time was 3600 s. The observations were obtained as a part of a survey of the SNRs in M81. SN 1993J was

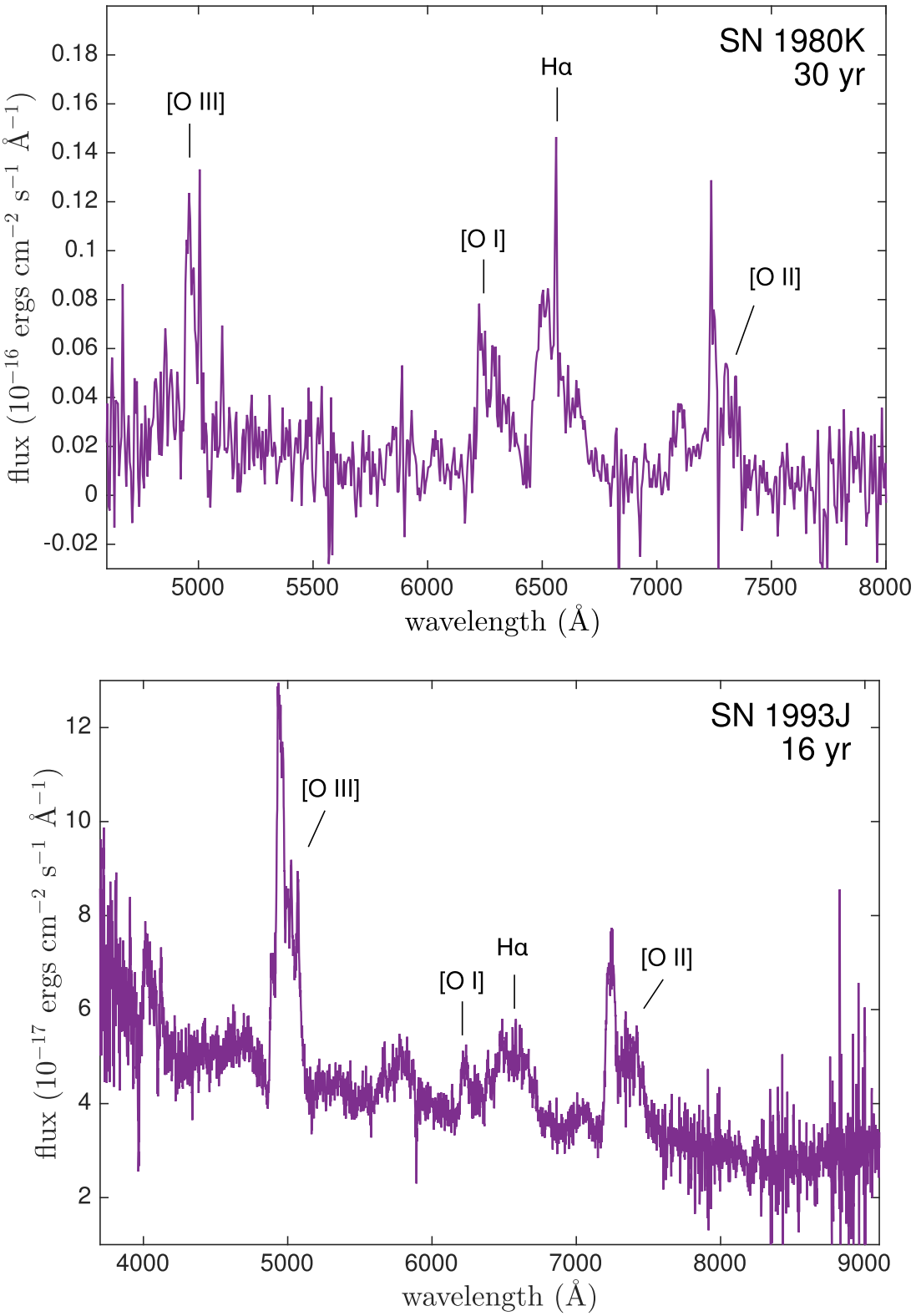

Figure 1. Above: the optical spectrum of SN 1980K on 2010 October 9 at 30 yr post-explosion. Below: the optical spectrum of SN 1993J on 2009 December 9 at 16 yr post-explosion. Both spectra were obtained by Milisavljevic et al. (2012).

approximately 16 yr old when the spectra were obtained. Many of the lines in its optical spectrum exhibit a flux bias towards the blue and also display noticeable substructure (see Fig. 1). They are generally broad and there is a significant degree of blending between lines. The lines least blended with other lines are those of [O III] λλ4959,5007 and [O II] λλ7319,7330 which both demonstrate significantly asymmetrical profiles, with both the flux and the peak of their profiles shifted towards the blue. The spectra have

been corrected for an M 81 velocity of -140 km s^{-1} (Matheson et al. 2000b).

Our modelling of SN 1980K focused on the Hα line and the [O I] $\lambda\lambda$6300,6363 Å doublet. Both of these line profiles exhibited a very strong blueshifted asymmetry indicative of the presence of dust in the ejecta and, like SN 1987A, were sufficiently distinct that they provided the best options for modelling purposes. Other lines were either too blended with each other or too noisy to be reliable.

SN 1993J exhibited its strongest line asymmetries in the oxygen lines, and in particular we focused our modelling on the [O II] $\lambda\lambda$ 7319,7330 and [O III] $\lambda\lambda$4959,5007 doublets mentioned above. The [O I] $\lambda\lambda$ 6300,6363 doublet was not modelled for SN 1993J as it was quite blended with the Hα line and the two features could not be easily separated. The [O II] and [O III] lines, being more distinct, were therefore the more sensible candidates for modelling.

Our approach to modelling the line profiles of both SN 1980K and SN 1993J followed the same principles as described for SN 1987A by Bevan & Barlow (2016). The maximum velocity was identified from the point at which flux vanishes on the blue side, the inner to outer radius ratio determined from various inflection points and the density profile was determined from the shape of the profile. We began the modelling by considering a smooth, coupled distribution of dust and gas before moving on to consider the effect on these models of adopting a clumped dust geometry whilst maintaining a smooth gas emissivity distribution. We first examined the line profiles in order to determine the maximum and minimum velocities before moving on to establish approximately the exponent of the dust and gas density distributions. Having fixed the starting values for these quantities, we iterated over the grain size and dust mass in order to fit the profile. We also occasionally varied the other parameters in order to optimize the fits to the data. We assumed that the oxygen doublets were optically thin for both SN 1980K and SN 1993J and using the theoretical transition probabilities detailed by Zeippen (1987) and Storey & Zeippen (2000) adopted a constant intrinsic flux ratio of 3.1 between the [O I] $\lambda\lambda$6300,6363 components, 1.2 between the [O II] $\lambda\lambda$7319,7330 components and 2.98 between the [O III] $\lambda\lambda$5007,4959 components. The intrinsic line profiles for SN 1980K and SN 1993J prior to dust effects both needed to be very 'boxy', that is, the ratio of the inner to outer radii is very high so that the overall profile has a very square shape (see Fig. 2). We present the intrinsic dust-free profile along with the best-fitting smooth Hα model for SN 1980K in the top panel of Fig. 2, along with the intrinsic dust-free profile, and the best-fitting smooth [O III] $\lambda\lambda$4959,5007 model for SN 1993J in the lower panel of Fig. 2.

The parameters for the smooth and clumped dust fits that we obtained for SN 1980K and SN 1993J are detailed in Tables 1 and 2, respectively. The smooth dust line profile fits for SN 1980K are presented in Fig. 3 and the clumped dust line profile fits are presented in Fig. 4. The smooth dust line profile fits for SN 1993J are presented in Fig. 5 and the clumped dust line profile fits are presented in Fig. 6.

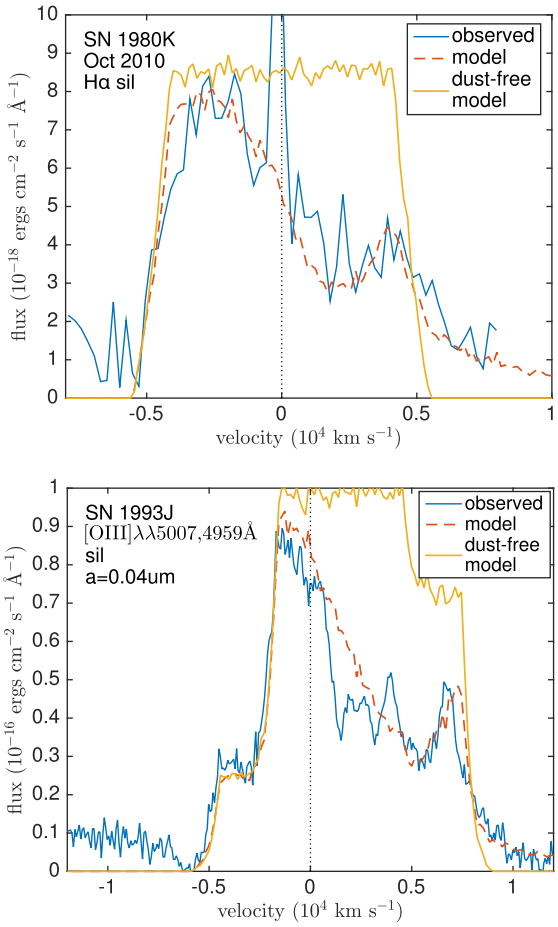

Figure 2. The best-fitting smooth dust models along with the intrinsic dust-free boxy profile for the Hα line profile for SN 1980K (upper) and the [O III] $\lambda\lambda$4959,5007 line profile for SN 1993J (lower). The intrinsic dust-free modelled line profile is given in yellow, the dust-affected modelled line profile in red and the observed line profile in blue.

3 MODELS FOR THE YEAR 30 LINE PROFILES OF SN 1980K

3.1 SN 1980K smooth dust models

We obtained good fits to both the Hα line and the [O I] $\lambda\lambda$6300,6363 doublet from SN 1980K (see Fig. 3). In particular, an extended wing on the red side of the profile was seen in both cases. This was more important for the Hα line since we could be sure that it was not a product of blending with an adjacent broad line (the presence of an extended red wing in the [O I] doublet may be due to blending with the blue wing of the Hα line). The Hα red wing allowed us to place constraints on the dust albedo using the approach described by Bevan & Barlow (2016). A high albedo of $\omega \approx 0.8$ was required to reproduce the flux in the region between $+6000$ and $+8000$ km s^{-1}. Astronomical silicate grains have a high albedo at 6563A (Hα), but amorphous carbon grain are never this reflective regardless of their size. As well as the best-fitting silicate model in Fig. 3, we include line profile fits using a large grain size ($a = 3.5$ µm) for amorphous carbon to generate as high an albedo as possible ($\omega \approx 0.6$) illustrating the slightly worse fit to the Hα line.

3.2 SN 1980K clumped dust models

Motivated by our modelling of SN 1987A (Bevan & Barlow 2016), we adopted a clumped dust structure with a clump volume filling factor of $f = 0.1$ and clumps of radius $R_{\rm clump} = R_{\rm out}/25$. All the dust was located in clumps but the gas emission remained distributed smoothly according to the distribution derived for the smooth models. A summary of the parameters for the best-fitting clumped models is presented in Table 1 and the fits are presented in Fig. 4.

Table 1. The parameters used for the smooth and clumped models of SN 1980K for media composed of 100 per cent amorphous carbon dust grains of radius 3.5 μm, or 100 per cent silicate dust grains of radius 0.1 μm. Optical depths are given from R_{in} to R_{out} at λ = 6300 Å for [O I] and λ = 6563 Å for Hα. The doublet ratio for [O I] λλ6300,6363 was fixed to be 3.1. Smooth dust models are listed in the first four rows and clumped dust models in the last four rows.

	Clumped?	Species	a (μm)	V_{max} (km s^{-1})	V_{min} (km s^{-1})	R_{in}/R_{out}	β	R_{out} (10^{17}cm)	R_{in} (10^{17}cm)	Doublet ratio	τ_λ	f	R_{clump} (10^{17}cm)	M_{dust} ($M_\odot$)
Hα	No	sil	0.1	5500	4125	0.75	2.0	5.2	3.9	–	1.41	–	–	0.10
Hα	No	amC	3.5	5500	4125	0.75	2.0	5.2	3.9	–	0.57	–	–	0.30
[O I]	No	sil	0.1	5500	4125	0.75	4.0	5.2	3.9	3.1	2.81	–	–	0.20
[O I]	No	amC	3.5	5500	4125	0.75	4.0	5.2	3.9	3.1	1.24	–	–	0.65
Hα	Yes	sil	0.1	5500	4125	0.75	2.0	5.2	3.9	–	1.68	0.1	0.2	0.12
Hα	Yes	amC	3.5	5500	4125	0.75	2.0	5.2	3.9	–	0.73	0.1	0.2	0.38
[O I]	Yes	sil	0.1	5500	4125	0.75	4.0	5.2	3.9	3.1	2.81	0.1	0.2	0.30
[O I]	Yes	amC	3.5	5500	4125	0.75	4.0	5.2	3.9	3.1	1.72	0.1	0.2	0.90

Table 2. The parameters used for the smooth and clumped year 16 models for SN 1993J for media composed of 100 per cent amorphous carbon dust grains of radius 3.5 μm, or 100 per cent silicate dust grains of radius 0.1 μm. Optical depths are given from R_{in} to R_{out} at λ = 7319 Å for [O II] and λ = 4959 Å for [O III]. Smooth dust models are listed in the first four rows and clumped dust models in the last four rows.

	Clumped?	Species	a (μm)	V_{max} (km s^{-1})	V_{min} (km s^{-1})	R_{in}/R_{out}	β	R_{out} (10^{17}cm)	R_{in} (10^{17}cm)	Doublet ratio	τ_λ	f	R_{clump} (10^{17}cm)	M_{dust} ($M_\odot$)
[O III]	No	sil	0.04	6000	4500	0.75	7	3.2	2.4	2.98	0.65	–	–	0.10
[O III]	No	amC	0.2	6000	4500	0.75	7	3.2	2.4	2.98	0.63	–	–	0.005
[O II]	No	sil	0.1	6000	4500	0.75	7	3.2	2.4	1.23	0.74	–	–	0.05
[O II]	No	amC	3.5	6000	4500	0.75	7	3.2	2.4	1.23	0.60	–	–	0.12
[O III]	Yes	sil	0.04	6000	4500	0.75	7	3.2	2.4	2.98	1.00	0.1	0.13	0.15
[O III]	Yes	amC	0.2	6000	4500	0.75	7	3.2	2.4	2.98	0.96	0.1	0.13	0.008
[O II]	Yes	sil	0.1	6000	4500	0.75	7	3.2	2.4	1.23	1.12	0.1	0.13	0.08
[O II]	Yes	amC	3.5	6000	4500	0.75	7	3.2	2.4	1.23	0.95	0.1	0.13	0.18

3.3 SN 1980K discussion

The models for the Hα and [O I] λλ6300,6363 profiles are broadly consistent with each other. The primary differences in their derived parameters (Table 1) are in the exponents of the density distributions and the total dust masses, with the oxygen distribution following a steeper density trend than the more diffusely emitted hydrogen. In a manner similar to the early phase models of SN 1987A, the [O I] λλ6300,6363 line profile models required significantly greater dust masses than the Hα models. We believe that this is likely to be due to the same reason discussed for SN 1987A by Bevan & Barlow (2016), namely that the dust-forming regions may be more concentrated towards those zones which are oxygen-rich (Kozma & Fransson 1998). As a result, it seems possible that if most of the gas-phase oxygen is located in clumps along with the dust then the discrepancy in the dust masses could potentially be resolved by considering more complex, decoupled distributions of dust and gas with diffuse hydrogen emission and clumped oxygen emission. Bevan & Barlow (2016) illustrated this possibility for SN 1987A. We note that for the clumped models for both SN 1980K and SN 1993J the difference between the dust masses derived from the [O I] λλ6300,6363 fits and Hα fits is around a factor of approximately 2, very similar to that seen for SN 1987A.

As discussed in Section 3.1 above, the Hα and [O I] line profiles of SN 1980K both exhibit an extended scattering wing which requires dust with a high albedo to fit it. Amorphous carbon models do not fit the red side of the Hα profile very well, even for very large grain sizes. We therefore adopt a silicate dust composition which fits the profiles somewhat better. We note that a combination of grain species would also be capable of producing the high albedo that is required but would be expected to result in dust masses somewhere in between those of the amorphous carbon and silicate models. The relatively low signal-to-noise ratio of both profiles means that a small degree of variation in the parameters is found to generate modelled line profiles that also fit the data reasonably. This is important for the determination of the high albedo which is based on a relatively small section of the observed line profile in the red wing of the data. Further observations with a higher signal-to-noise ratio could be beneficial.

There has been only limited discussion of the dust mass that could be present in the ejecta of SN 1980K other than that dust must be present based on the asymmetrical optical line profiles. The initial evidence for dust in the ejecta of SN 1980K was based on the near-IR flux excess seen a few hundred days after outburst (Dwek et al. 1983). They discussed the possibility of newly formed dust in the ejecta accounting for this IR flux but also acknowledged the possibility that the excess IR flux could also be a product of the reheating of pre-existing dust grains in circumstellar material. Sugerman et al. (2012) presented detailed modelling of the light echoes of SN 1980K and concluded that thermal echoes off a thin circumstellar shell of dust, of light emitted from an ultraviolet flash in the first 2 d, or optical light emitted in the first 150 d, were contributing to the observed IR flux but could account only for a small fraction of that flux. Whilst circumstellar dust may in fact explain the early IR emission, dust located in a circumstellar shell outside the SN ejecta cannot explain the observed asymmetries in the late-time optical line profiles.

Other explanations for the stubborn presence of strongly blueshifted asymmetrical optical lines have been advanced previously for SN 1980K. Fesen & Becker (1990) argued that broad asymmetrical lines in the early spectra could arise as a result of the impact between the blast wave and pre-existing circumstellar

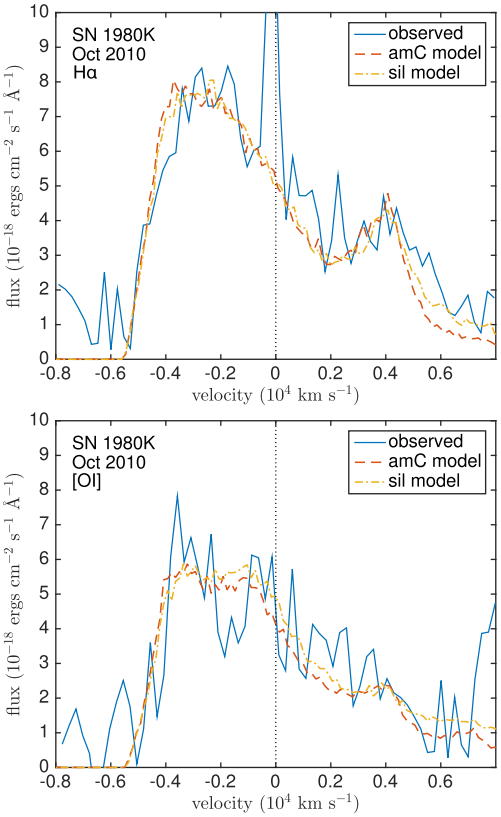

Figure 3. Best smooth dust fits for the SN 1980K Hα line (upper) and for the [O I] $\lambda\lambda$6300,6363 doublet (lower) for the parameters detailed in Table 1. Smooth dust fits with astronomical silicate grains of radius $a = 0.1$ μm are presented in yellow and smooth dust fits with amorphous carbon grains of radius $a = 3.5$ μm in red. For the [O I] doublet, zero velocity was set at $\lambda = 6300$ Å.

material. Similarly, a 'clumpy wind' model with emission coming from shocked clumps in order to explain the blueshifted lines was put forward by Chugai & Danziger (1994). Both of these mechanisms could theoretically result in asymmetrical line profiles as a result of the emission from the approaching side of the SN ejecta reaching us before emission from the receding side. However, both of these suggestions were ruled out by Sugerman et al. (2012) based primarily on analyses of the various time-scales involved but also on their inability to reproduce the observed late-time excess IR flux. Fesen & Becker (1990) also noted the possibility of blueshifted lines arising as a result of dust forming in the ejecta but were doubtful as to the feasibility of the diffusely emitted hydrogen being so strongly affected by dust forming in the more dense, central regions of the ejecta. Sugerman et al. (2012) estimated that a dust mass of $\sim 10^{-3}$ M$_\odot$ was needed to explain the mid-IR spectral energy distribution at similar epochs (23–30 yr post-outburst) to those investigated here, with the presence of as much as a few M$_\odot$ of cold dust possible due to the fact that the SED was still rising at 24 μm. This latter possibility was noted based on the depth to which *Herschel* could probe during far-IR observations of NGC 6946 in 2010. A few M$_\odot$ of cold dust in the ejecta of SN 1980K would not have been detected by *Herschel*. These results, though not particularly constraining, are consistent with our current estimates that up to 0.9 M$_\odot$ of dust can be present in the ejecta of SN 1980K. Given the strong oxygen forbidden lines in the spectrum of SN 1980K, a silicate-dominated dust composition, rather than amorphous carbon, seems likely, implying a clumped dust mass of between 0.12 and 0.30 M$_\odot$ at year 30 (Table 1).

4 MODELS FOR THE YEAR 16 LINE PROFILES OF SN 1993J

4.1 SN 1993J smooth dust models

We had mixed success in obtaining good fits to the oxygen line profiles of SN 1993J. Certain aspects of the line profiles are well fitted by the models, such as the bump seen at -4000 km s^{-1} in the frame of [O III] λ4959. The peaks of the [O III] profile were fairly well matched although we could not exactly reproduce the peak seen at $+4000$ km s^{-1} (Figs 5 and 6). Similarly, we struggled to reproduce the shape of the profile between -2000 and $+2000$ km s^{-1} for both the [O III] and [O II] doublets. In order to fit the profile, we needed to use different-sized grains for the [O III] and the [O II] models in order to fit the red wings of the profiles. Parameters for the smooth dust models for [O III] $\lambda\lambda$4959,5007 and [O II] $\lambda\lambda$7319,7330 that are presented in Fig. 5 are detailed in Table 2.

4.2 SN 1993J clumped dust models

Our clumped dust models for SN 1993J adopt the same clumped structure as for the SN 1980K clumped models and the SN 1987A

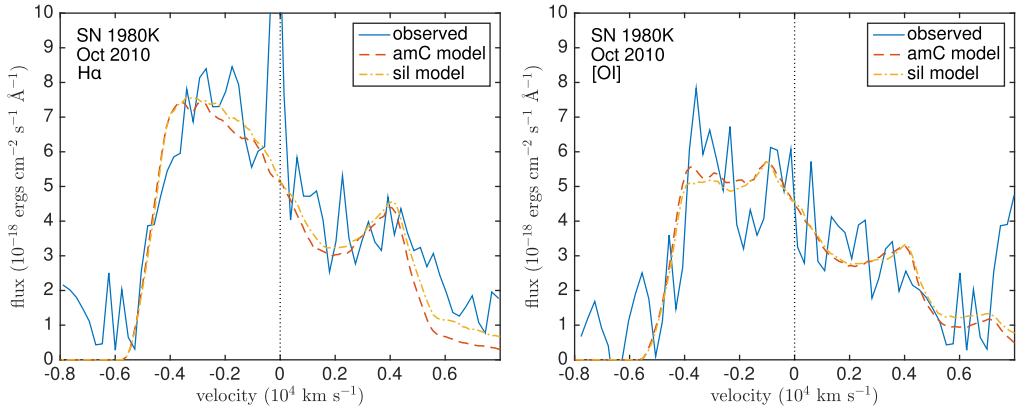

Figure 4. Best clumped dust fits to the SN 1980K Hα line (top) and the [O I] $\lambda\lambda$6300,6363 doublet (bottom) for the parameters detailed in Table 1. Clumped dust fits with astronomical silicate grains of radius $a = 0.1$ μm are presented on the left and clumped dust fits with amorphous carbon grains of radius $a = 3.5$ μm are presented on the right. For the [O I] doublet, zero velocity was set at $\lambda = 6300$ Å.

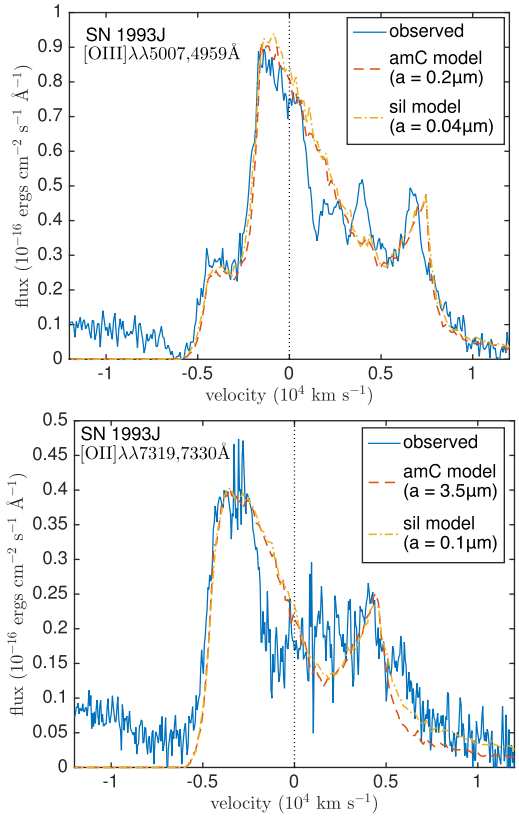

Figure 5. Best smooth dust fits to the year 16 SN 1993J [O III] λλ4959,5007 doublet (top) and the [O II] λλ7319,7330 doublet (bottom) for the parameters detailed in Table 2. For the [O II] doublet, zero velocity was set at λ = 7319 Å and for the [O III] doublet, zero velocity was set at λ = 4959 Å. Compositions and grain sizes are as detailed on the plots.

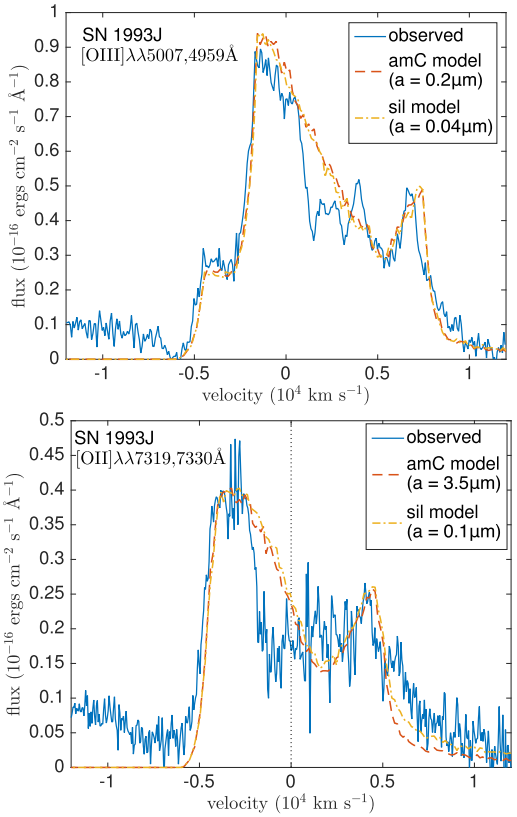

Figure 6. Best clumped dust fits to the Year 16 SN 1993J [O III] λλ4959,5007 doublet (top) and the [O II] λλ7319,7330 doublet (bottom) for the parameters detailed in Table 2. For the [O II] doublet, zero velocity was set at λ = 7319 Å and for the [O III] doublet, zero velocity was set at λ = 4959 Å. Compositions and grain sizes are as detailed on the plots.

clumped models ($f = 0.1$ and $R_{\rm clump} = R_{\rm out}/25$). All of the parameters were kept fixed from the smooth models except for the new clumped dust distribution. Similar fits were found and the clumped geometry had little effect on the resultant modelled line profiles. The required dust mass increased by a factor of approximately 1.5. The clumped model parameters for the [O III] λλ4959,5007 and [O II] λλ7319,7330 fits that are presented in Fig. 6 are detailed in Table 2.

4.3 SN 1993J discussion

Our models for the optical line profiles of SN 1993J do not fit the observed data quite as well as the models for the other objects. In particular, the modelled profiles tend to overestimate the flux in the region just to the red side of the peak flux, where the observed profile exhibits a sharp downturn (see Fig. 2). The steepness of this drop cannot be matched by the models. However, certain other features of the observed profiles are fitted well by the model. For example, the [O III] λλ4959,5007 model line profile in particular fits bumpy features on both the red and blue sides of the profile at approximately -4000 km s^{-1} and $+6000$ km s^{-1} quite well. The bump near $+6000$ km s^{-1} is simply due to absorption in the region between $-V_{\rm min}$ and $+V_{\rm min}$ causing a peak at the location of the minimum velocity (for the 5007 Å component). The small discrepancy in the location of the [O III] peak at around $\sim+6000$ km s^{-1} may be a result of a net velocity shift of the SN away from the observer (see Section 5.2 for a discussion of such effects in more detail) or a discrepancy between the adopted smooth, symmetrical gaseous emission models and a more clumpy, asymmetrical geometrical structure for the remnant (Tran et al. 1997). Similarly, the difference in grain sizes, and hence dust masses, required to fit the [O III] and [O II] lines (see Table 2) may also indicate the need for a different distribution of dust or gas. The bumpy features seen in these lines were discussed by Matheson et al. (2000b), who postulated that the 'double-horned' shape was a consequence of the ejecta colliding with a disc-like or flattened region. While it is possible that the blueshifted asymmetry observed in the optical line profiles is not a result of dust in the ejecta, given how well certain aspects of the observed profiles are fitted, it seems more likely that it is simply the case that a more complex emission geometry is required for the models to better fit the data.

A manual investigation of parameter space suggested that the issues with fitting the shapes of the profiles derived from the initial emissivity distribution. The smooth nature of the emissivity distribution that we adopted could not reproduce the sharp downturn seen to the red side of the peak flux. This could be due to an oxygen emission distribution that is potentially composed of a dense central region that produces the steep variations in the central regions, with a more diffuse oxygen envelope accounting for the wings.

Nozawa et al. (2010) have presented post-explosion elemental abundance profiles computed for an analogue of a Type IIb SN (such as Cas A or SN 1993J), with an initial mass of 18 $M_\odot$ and a residual stellar mass of 4.5 $M_\odot$ at the time of explosion. Oxygen was predicted to be the dominant element in the inner 1.1 $M_\odot$ of the 2.9 $M_\odot$ ejecta, and to have a significant abundance in the 1.3 $M_\odot$

layer above that (O/He $\sim 3 \times 10^{-3}$, but with a C/O ratio of ∼2.5). Our overestimation of the flux just to the red side of the peak might be resolved by considering a two-component density–velocity distribution such as this. SN 1993J had a particularly unusual red supergiant progenitor with a postulated stripped envelope caused by the presence of a B-star binary companion (Maund et al. 2004; Fox et al. 2014) resulting in a significant mass of circumstellar material surrounding the progenitor star. Photometric analyses performed by Zhang et al. (2004) suggested that the late-time optical emission from SN 1993J is largely powered by interaction between the blast wave and the circumstellar material. In this case, the geometry of the emitting regions is especially complex, and may in particular account for the significant substructure seen in the optical line profiles.

For both SN 1980K and SN 1993J, the effects of including a clumped dust distribution in the models rather than a smooth dust distribution increased the required dust mass by a factor of approximately 1.5, very similar to the factor found for SN 1987A from the models presented by Bevan & Barlow (2016). In these cases, the clumped geometry has little effect on the resulting profiles except to reduce the degree of absorption. The extent of the extended red scattering wing is also somewhat reduced by dust clumping. Since SN 1993J's spectrum is dominated by oxygen lines, we prefer our silicate dust models to those that used amorphous carbon, implying a clumped dust mass of 0.08–0.15 $M_\odot$ for SN 1993J at year 16 (Table 2).

5 CASSIOPEIA A

Cassiopeia A (Cas A) is a young SNR at an estimated distance of 3.4 kpc (Reed et al. 1995). The X-ray radii of the reverse and forward shocks measured by *Chandra* were 95 ± 10 and 153 ± 12 arcsec (Gotthelf et al. 2001), corresponding to physical radii of 1.57 and 2.52 pc, respectively. Analysis of its expansion velocities and geometry have allowed the explosion date to be estimated as 1681 ± 19 CE (Fesen et al. 2006), implying that the remnant was approximately 330 yr old at the time that the spectra discussed here were obtained. Cas A is the strongest radio source in the sky outside of the Solar system and has been comprehensively observed across the electromagnetic spectrum. Optical spectroscopy of light echoes from the SN scattered off surrounding interstellar dust has allowed the original SN explosion to be spectroscopically classified, leading to the conclusion that Cas A was the result of a Type IIb SN explosion (Krause et al. 2008).

Arendt, Dwek & Moseley (1999) estimated a mass of 0.038 $M_\odot$ of 52 K dust in Cas A based on fitting *IRAS* 60 and 100 μm fluxes. From *Spitzer* IRS spectroscopy and MIPS photometry, Rho et al. (2008) estimated that a mass of 0.020–0.054 $M_\odot$ of warm 65–265 K dust was emitting between 5 and 70 μm, particularly in a bright ring associated with the reverse shock. Arendt et al. (2014) used *Spitzer* IRS spectra and PACS 70–160-μm photometry to estimate a mass of ∼0.04 $M_\odot$ of warm dust in Cas A.

Observations at longer wavelengths of the cold dust in the ejecta have led to higher dust mass estimates, with Dunne et al. (2003) using SCUBA 450- and 850-μm photometry to estimate a dust mass of 2–4 $M_\odot$. This was contested by Krause et al. (2004), who suggested that the majority of the dust emission originated from cold interstellar clouds located along the line of sight to Cas A and placed an upper limit of 0.2 $M_\odot$ of cold dust in the ejecta. However, observations of strongly polarized 850-μm emission obtained using the SCUBA polarimeter have been used to argue for the presence of an ejecta-condensed cold dust mass of ∼0.9 $M_\odot$ (Dunne et al. 2009).

Modelling by Nozawa et al. (2010) reproduced the observed *IRAS*, *ISO* and *Spitzer* IR SED using 0.08 $M_\odot$ of dust, of which 0.072 $M_\odot$ was inside the radius of the reverse shock. Sibthorpe et al. (2010) used far-IR and sub-mm *AKARI* and balloon-borne BLAST observations to estimate a 35 K dust mass of 0.06 $M_\odot$ in Cas A, while Barlow et al. (2010) used higher angular resolution *Herschel* PACS and SPIRE photometry to estimate a mass of 0.075 ± 0.028 $M_\odot$ of $T \sim 35$ K silicate dust located mainly inside the reverse shock, which combined with the previously estimated mass of 0.02–0.05 $M_\odot$ of warmer dust associated with the reverse shock yielded a total dust mass estimate of ∼0.1 $M_\odot$ for Cas A.

5.1 The integrated optical spectrum of Cas A

The integrated optical spectrum of Cas A, obtained by Milisavljevic & Fesen (2013) and discussed by Milisavljevic et al. (2012), is displayed in Fig. 7. It shows red–blue asymmetries in many of the line profiles. In particular, the oxygen lines [O I] λλ6300,6363, [O II] λλ7319,7330 and [O III] λλ4959,5007 exhibit a blueshifted asymmetry, with the [O III] doublet especially demonstrating a strong blueshift with considerable substructure. We have modelled all three of these features with a primary focus on the [O III] doublet.

The integrated spectrum was composed of observations carried out mainly in 2007 September and 2008 September at Kitt Peak, Arizona using the MDM 2.4m Hiltner telescope, as described by Milisavljevic & Fesen (2013). The MDM Modular Spectrograph was used with a 2048 × 2048 CCD detector and a long slit of dimensions 2 arcsec × 5 arcmin oriented North–South. Exposure times were generally 2 × 500 s. The wavelength range covered was 4500–7000 Å with a spectral resolution of 6 Å. The integrated spectrum was ultimately composed of 80 long slit spectra spaced 3 arcsec apart across the entire main shell. The slit positions are shown in fig. 1 of Milisavljevic & Fesen (2013).

5.2 Smooth dust models for the oxygen lines of Cas A

The modelling of the Cas A spectrum was initially focused on the [O III] λλ4959,5007 doublet, which exhibits a pronounced asymmetry. The process of finding a fit to the line profile was the same as described earlier. The maximum velocity was identified from the point at which flux vanishes on the blue side, the inner to outer radius ratio was determined from various inflection points and the density profile was determined from the shape of the profile. The other parameters were then iterated to find the best-fitting profile.

We initially produced a fit to the data using the parameters listed in the first row of Table 3. The profile is presented in the top panel of Fig. 8. As can be seen, the modelled line profile fits most of the observed line profile, but fails to fit the red side of the profile adequately. A thorough, manual investigation of parameter space resulted in the conclusion that the profile was much better fitted if the entire modelled profile was shifted to the red by +700 km s^{-1}. There is other evidence in favour of this assumption. The dynamics of Cas A are known to be significantly asymmetrical (Rest et al. 2011), with radial velocities spanning −4000 to +6000 km s^{-1} (Milisavljevic & Fesen 2013) suggesting that the net line-of-sight velocity is likely away from the observer and indicating the need for an overall velocity shift to correct for this. Using *Spitzer* IRS 5–40-μm spectra to construct a 3D model of the remnant, DeLaney et al.

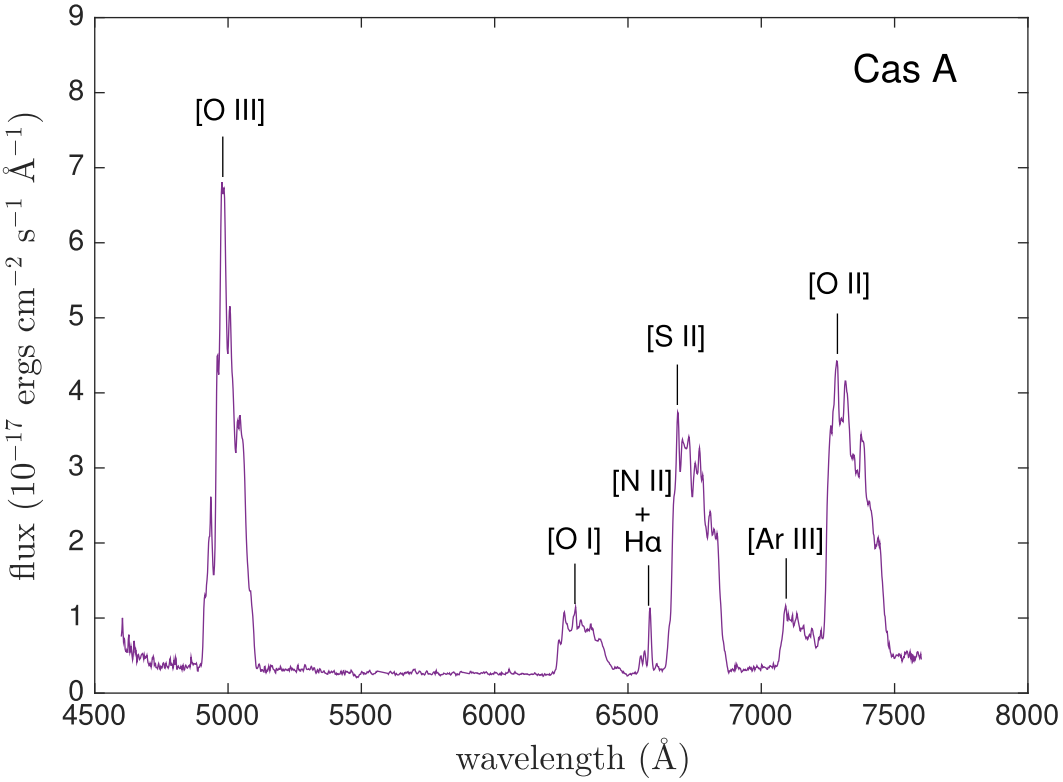

Figure 7. The integrated spectrum of Cas A – see Milisavljevic & Fesen (2013) and Section 5.1.

Table 3. The parameters used for the smooth models of Cas A with a medium composed of 50 per cent amorphous carbon and 50 per cent silicate grains of radius $a = 0.05\,\mu$m. Dust optical depths are given from R_{in} to R_{out} at $\lambda = 5007$ Å for [O III], $\lambda = 7319$ Å for [O II] and $\lambda = 6300$ Å for [O I]. The doublet ratio is always the ratio of the stronger line to the weaker line. The asterisk indicates that the parameters listed describe the gas density distribution. The dust density distribution is the same in all cases (as detailed for the shifted [O II] doublet in the second row).

	v shift (km s^{-1})	V_{max} (km s^{-1})	V_{min} (km s^{-1})	R_{in}/R_{out}	β	M_{dust} ($M_\odot$)	R_{out} (10^{18}cm)	R_{in} (10^{18}cm)	Doublet ratio	τ_λ
[O III]	0	4500	1800	0.4	2.0	0.9	4.7	1.9	2.98	0.53
[O III]	+700	5000	2500	0.5	2.0	1.1	5.2	2.6	2.98	0.49
[O II]*	+1000	5000	3250	0.65	2.0	1.1	5.2	3.4	1.23	0.21
[O I]*	+1000	5000	3250	0.65	2.0	1.1	5.2	3.4	3.1	0.30

(2010) derived an average velocity offset away from the observer of +859 km s^{-1}. From their optical reconstruction of the remnant, Milisavljevic & Fesen (2013) derived an offset of +760 ± 100 km s^{-1} that is consistent with our own estimate.

We found that models of the [O II] λλ7319,7330 and [O I] λλ6300,6363 lines were also substantially improved if the entire model profile was allowed to be uniformly shifted towards the red. For the remainder of the models, we therefore shifted the profiles in velocity space to better fit the data based on the likelihood that the sampled emitting regions had an overall net velocity away from the observer. Fits to the line profiles were significantly improved following this translation.

A model with the shifted [O III] λλ4959,5007 line is presented in Fig. 8 for a dust medium composed of 50 per cent amorphous carbon and 50 per cent silicate grains of radius $a = 0.05\,\mu$m. The parameters used for this model are presented in the second row of Table 3. A total dust optical depth of $\tau = 0.49$ at 5007 Å between R_{in} and R_{out} was found to best fit the profile. An albedo of $\omega \approx 0.15$ at 5007 Å was needed to match the flux on the far red side of the model profile to that observed.

The composition of the dust has a significant effect on the overall dust mass for this optical depth and albedo. An attenuated line profile model of the [O III] λλ4959,5007 doublet from Cas A could not be found using 100 per cent astronomical silicate dust (Draine & Lee 1984). There is little to no red scattering wing seen, hence the relatively low value of ω, and therefore relatively small silicate grains would be required to reproduce the red side of the profile. Silicate grains of this size have extremely low optical absorption efficiencies and therefore the best-fitting optical depth of $\tau = 0.49$ would correspond to an implausibly large mass of dust (>20 $M_\odot$) if it was composed entirely of astronomical silicates.

The chemical composition of the dust in the ejecta of Cas A is known to be extremely complex (Rho et al. 2008; Arendt et al. 2014) with many different species of dust grain present in the ejecta. The presence of silicate dust has been deduced based on the silicaceous emission features observed in the mid-IR region of the spectrum (Rho et al. 2008). However, the potential presence of a variety of other species has been discussed (Arendt et al. 2014). In Table 4, we detail the dust masses required to fit the [O III]λλ4959,5007 line profile for different fractions of silicates and amorphous carbon

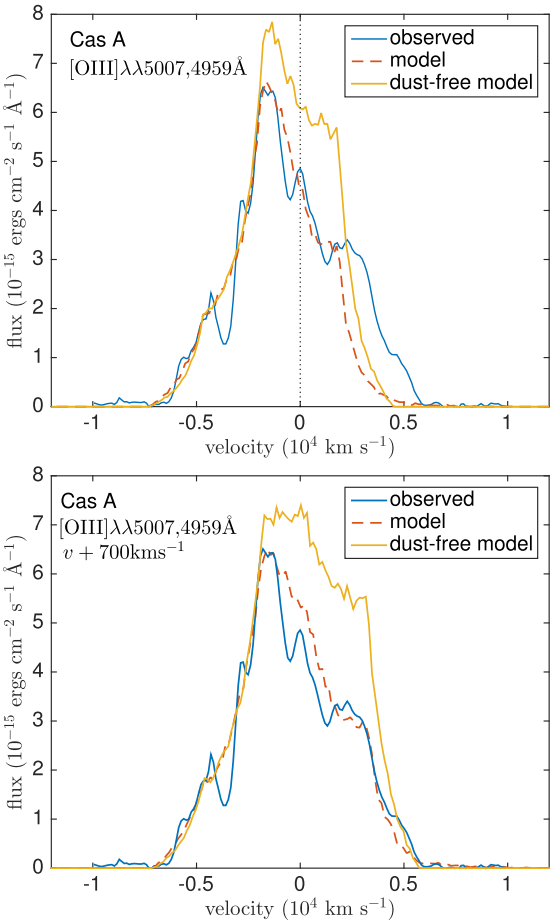

Figure 8. Best smooth dust fits to the Cas A [O III] λλ4959,5007 doublet for the parameters detailed in Table 3, along with the modelled intrinsic line profile (yellow). The top plot shows an unshifted fit to the [O III] line profile and in the bottom plot the model [O III] line has been shifted uniformly towards the red by +700 km s^{-1}. Zero velocity was set at λ = 4959 Å.

Table 4. The variation in dust mass for a fixed dust optical depth $\tau_{5007} = 0.49$ for the smooth dust parameters listed in Table 3.

per cent silicate grains	per cent amorphous carbon grains	Grain radius a (μm)	$M_{\rm dust}$ ($M_\odot$)
90	10	0.035	6.5
75	25	0.04	2.5
50	50	0.045	1.1
25	75	0.048	0.6
0	100	0.05	0.37

grains for a single grain size. For each composition, we determined the grain radius based on the albedo necessary to fit the profile ($\omega \approx 0.15$) and then varied the dust mass to achieve the required optical depth. The derived dust masses cover a wide range of values, between 0.37 and 6.5 $M_\odot$.

We investigated whether it was possible to determine the approximate dust composition based on the relative optical depths necessary to fit different blueshifted lines in the spectrum and the wavelength dependence of dust absorption for different grain compositions and sizes. We therefore considered the blueshifted [O II] λλ7319,7330 and [O III] λλ4959,5007 Å lines from Cas A. Unfortunately, at the small grain sizes required, there is no significant variation between the absorption efficiencies at 5007 and 7319 Å for different dust

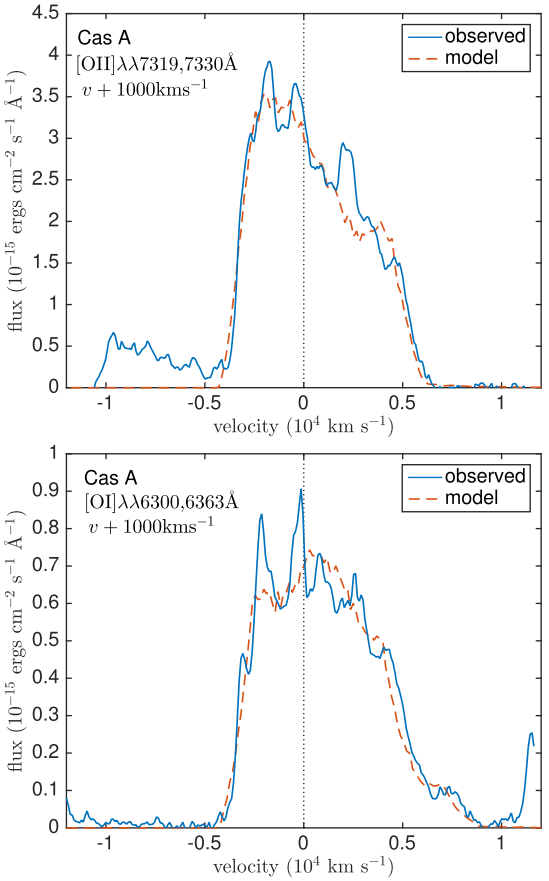

Figure 9. Best smooth dust fits to the Cas A [O II] λλ7319,7330 doublet (top) and the [O I] λλ6300,6363 doublet (bottom) for the parameters detailed in Table 3. Both model line profiles have been shifted uniformly towards the red by +1000 km s^{-1}.

compositions and we could not therefore determine the composition via this approach. Additionally, the [O II] and [O I] lines are much less sensitive to variations in the density distributions and the dust mass, partly due to the high frequency of bumpy features observed in these lines which contaminate the intrinsic broad profile. The best-fitting models for these lines were therefore quite degenerate, i.e. there were multiple sets of parameters that resulted in reasonable fits.

However, it was possible to use these lines to determine the reliability of the best-fitting model for the [O III] λλ4959,5007 line profile. We adopted the dust distribution determined using the [O III] fits and investigated models for the [O II] λλ7319,7300 and [O I] λλ6300,6363 profiles to see if this dust distribution was capable of fitting these lines as well. We adopted an emissivity distribution that was slightly different to the [O III] line (see Table 3) and shifted the observed line profiles by −1000 km s^{-1}. These emissivity distributions were then modelled with the dust distribution and dust mass for the best-fitting smooth [O III] model. The resultant [O II] and [O I] line profiles can be considered good fits (see Fig. 9). This suggests that the models are consistent and, if the relative abundances of the dust grain species present in the ejecta can be determined via other means, that the dust mass can be well constrained using this method. As in the cases of the line profile fitting for SN 1980K and SN 1993J, all of the line profile models listed above adopted intrinsic doublet strengths from Zeippen (1987) and Storey & Zeippen (2000).

Table 5. The ratio of clumped dust mass to smooth dust mass for the model whose parameters are given in Row 2 of Table 3, for clumped models with different clump widths and different clump volume filling factors. The other parameters in the models were fixed at the values given in Table 3.

Clump radius	$f = 0.05$	$f = 0.1$	$f = 0.25$
$R_{out}/10$	3.5	1.9	1.4
$R_{out}/25$	1.6	1.0	1.0

5.3 Clumped dust models for the oxygen lines of Cas A

Cas A is highly clumped (Fesen et al. 2001). Recently, models by Biscaro & Cherchneff (2014) have suggested that dust cannot in fact form in the gas phase in the ejecta of Cas A unless extremely dense knots of material are present. It is therefore important, as with SN 1987A, to consider the effects of dust clumping on the line profiles. We continue to focus on the [O III] line profile from Cas A in considering the effects of clumping. Clearly, the ejecta have a complex geometry with many clumps of different sizes and potentially different ionization states and dust species within each. The models that we present here are included to give some indication of the effects of clumping within the ejecta rather than to be representative of the state of the ejecta at this time. To this end we present a number of models of the [O III] line profile based on the smooth dust fits that we presented in the previous section. We consider two different clump sizes, ones with width $R_{out}/25$ and ones with width $R_{out}/10$. We also consider three different clump volume filling factors $f = 0.05$, $f = 0.1$ and $f = 0.25$. For each combination of clump size and filling factor, we evaluated the required increase or decrease in the dust mass over the smooth dust model. All other parameters were kept fixed so that line packets were emitted according to the smooth distribution and geometry described by the parameters listed in Table 3.

The factor by which the required dust mass changes relative to the smooth dust mass is listed in Table 5 (i.e. relative to $M_{dust} = 1.1$ M$_\odot$ for a medium of 50 per cent astronomical silicates and 50 per cent amorphous carbon; see Table 4 for other dust masses with different dust compositions). Whilst clumping serves to increase the required dust mass in most cases, in the most extreme case it is still only by a factor of ∼3.5. The fits for all of these cases are presented in Fig. 10.

5.4 Cas A discussion

The models of Cas A adopt a maximum expansion velocity of ∼5000 km s^{-1} which gives an outer radius of 5.2×10^{18} cm (1.69 pc), i.e. just beyond the reverse shock radius of 1.57 pc (Gotthelf et al. 2001). The need to shift the profiles by either −700 km s^{-1} or −1000 km s^{-1} in order to fit them is consistent with the IR line expansion velocity asymmetry observed by DeLaney et al. (2010); an offset of 1000 km s^{-1} applied to an originally symmetrical distribution between −5000 and +5000 km s^{-1} results in the velocity range that they deduced. DeLaney et al. (2010) derived an average velocity offset away from the observer of +859 km s^{-1}, midway between the 700 and 1000 km s^{-1} velocity offsets that we adopt for the [O III] line and for the [O I] and [O II] lines, respectively. Additionally, from their analysis of the projected velocities of the optical emission line knots in Cas A, Milisavljevic & Fesen (2013) deduced an overall asymmetry of +760 ± 100 km s^{-1}.

The structure of the Cas A remnant is much more complex than the simple shell geometry adopted here; it exhibits large-scale coherent structure (DeLaney et al. 2010). The majority of the optical ejecta are arranged in several well defined and nearly circular filaments with diameters between approximately 30 arcsec (0.5 pc) and 2 arcmin (2 pc, see e.g. fig. 7 of Milisavljevic & Fesen 2013). These filaments are the likely cause of the noticeable bumpy substructure of the observed emission lines that we model here. The models that we have presented above represent a first-order approximation to the geometry of Cas A; future work will hopefully include a more realistic density distribution based on line emissivity distributions derived from observations.

It is not just the geometrical structure of the Cas A remnant that is complex (Rho et al. 2008; Arendt et al. 2014; Biscaro & Cherchneff 2014). Arendt et al. (2014) concluded that the entire spectrum of Cas A can be fitted using only four dust species: $Mg_{0.7}SiO_{2.7}$, $Mg_{2.4}SiO_{4.4}$, Al_2O_3 and amorphous carbon. Two of these species ($Mg_{0.7}SiO_{2.7}$, $Mg_{2.4}SiO_{4.4}$) are highly scattering and two (Al_2O_3 and amorphous carbon) are relatively absorbing. This suggests that dust composition models with both silicates and amorphous carbon may be the most representative. Whilst there is evidence for a number of grain species in the warm dust component, the cool dust component, found by Barlow et al. (2010) and the subject of a recent spatially resolved analysis by De Looze et al. (2016), constitutes the majority of the dust in Cas A but is of still unknown composition.

The most likely dust mass of ∼1.1 M$_\odot$ for Cas A given by our modelling is higher than the recent estimates of the dust mass present in Cas A that were discussed at the start of this section. However, it is consistent with the recent estimate (De Looze et al. 2016) of a mass of 0.4–0.7 M$_\odot$ of cold dust in Cas A, based on a spatially resolved analysis of *Spitzer* and *Herschel* imaging photometry from 20 to 500 μm that accounted for contributions from interstellar dust and from SN synchrotron and dust emission components. Further line profile models of Cas A that adopt a more realistic and complex geometry for both the gas and dust may help to constrain its total dust mass further.

6 CONCLUSIONS

Of a sample of 10 CCSNe that were still visible spectroscopically at late times, at least 50 per cent exhibited blueshifted line profiles (Milisavljevic et al. 2012). This aspect of the optical spectra of CCSNe at late times is most simply explained by the presence of dust in the ejecta. We have modelled oxygen and hydrogen line profiles in the optical spectra of three SNRs with ages of ∼16, 30 and 330 yr and have found that we can reproduce the observed line profiles fairly well even with relatively simple models. Further modelling that allows for more complex emission geometries may allow even better fits to be obtained. Regardless, it seems clear that the presence of newly formed dust in the ejecta of these objects can account for the frequently seen blueshifting of their line profiles.

We find that for SN 1980K a high albedo is required to fit the red wing of the line profiles and that the dust composition is therefore likely dominated by silicate grains. We obtain a dust mass in the range 0.1–0.3 M$_\odot$ at 30 years post-explosion. In the case of SN 1993J, a dust mass of between 0.08 and 0.15 M$_\odot$ at 16 yr post-outburst is derived based on a silicate dust model. In both cases, a clumped dust model requires approximately 1.5 times as much dust as a smooth dust model. In the case of Cas A, asymmetries in the ejecta require the modelled profiles to be shifted by ∼700–1000 km s^{-1}. The dust mass in Cas A is not tightly constrained since the dust composition cannot be determined. However, a likely composition comprises a mixture of reflective and

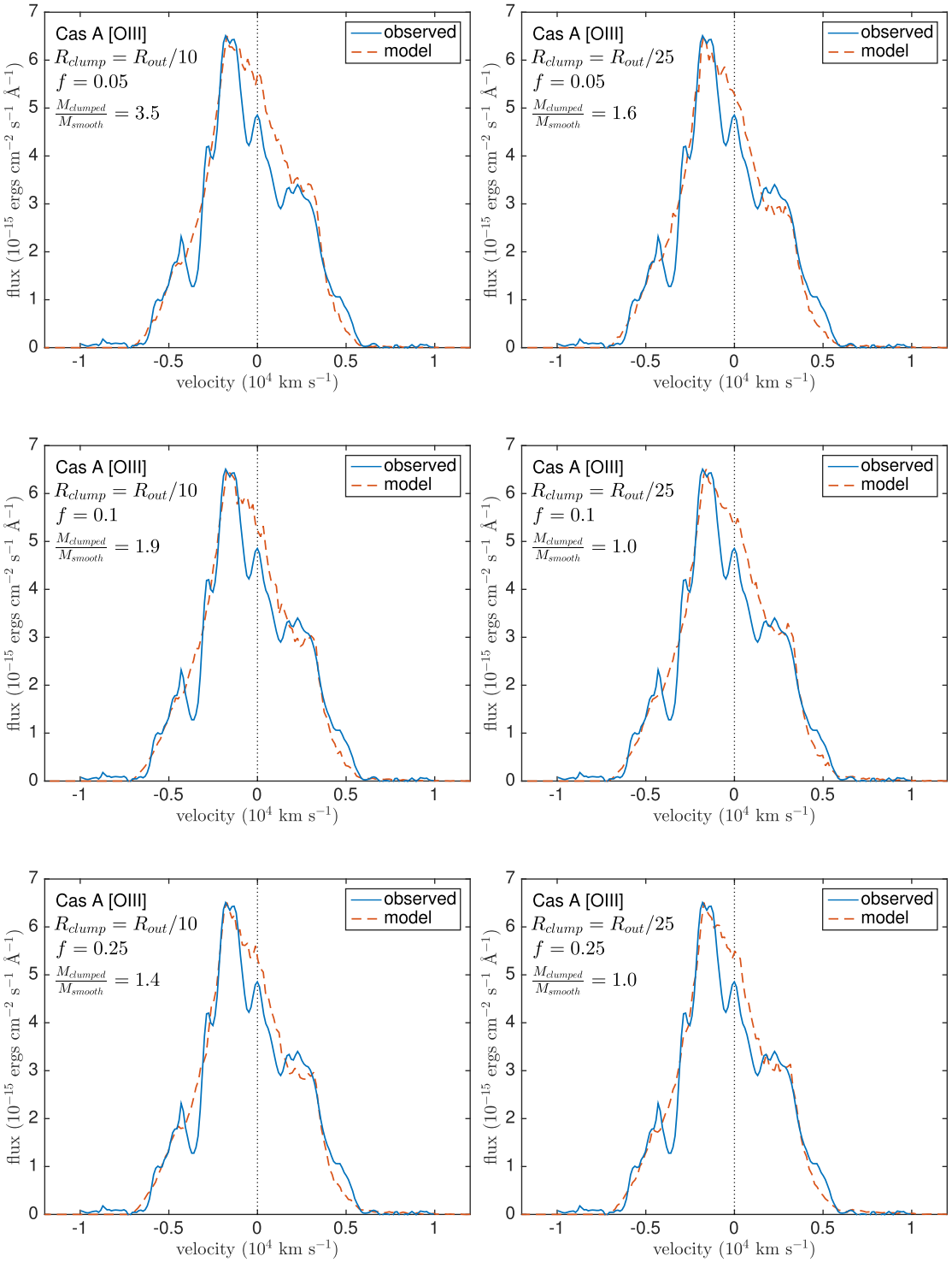

Figure 10. Best clumped dust fits to the Cas A [O III] λλ4959,5007 doublet for the parameters described in Tables 3 and 5. In the left column are fits to the profile using clumps with $R_{\rm clump} = R_{\rm out}/10$ and in the right column are fits using clumps with $R_{\rm clump} = R_{\rm out}/25$. Each row uses a model that adopts a different clump volume filling factor with $f = 0.05$ on the top, $f = 0.1$ in the middle and $f = 0.25$ on the bottom. The model profile has been shifted uniformly towards the red by +700 km s^{-1}.

absorbing grains. A mixture of 50 per cent silicate grains and 50 per cent amorphous carbon grains by number yields a dust mass of 1.1 $M_\odot$.

Our aim throughout the modelling of these three objects has been to investigate the feasibility that dust causes the red-blue asymmetries observed in the optical line profiles from CCSNRs and then to determine the dust masses that cause these characteristic dust-affected line profiles. Whilst the derived dust masses are dependent on clumping structures and dust composition, at these late stages we find that significant dust optical depths (typically 0.5–2) and large dust masses (0.1–1.1 $M_\odot$) are required to account for the degree of blueshifting observed.

Gall et al. (2014) brought together a number of CCSN dust mass estimates from the literature, based largely on IR SED fitting, across a range of epochs up to ∼25 yr. When they plotted dust masses as a function of time since the CCSN explosion, they found a steady increase. Separately, Wesson et al. (2015) plotted IR- and submillimetre-based dust mass estimates for SN 1987A from day 615 to year 25 and found a similar trend of increasing dust mass with time, from 0.001 ± 0002 $M_\odot$ at day 615 to 0.7 ± 0.1 $M_\odot$ at years 23–25. The dust masses derived by Bevan & Barlow (2016) from SN 1987A's line asymmetries up to year 10 filled in some of the gaps left by the IR/submm SED studies and confirmed the trend of increasing dust mass with time. Our dust mass estimates for SN 1993J at year 16 (0.08–0.15 $M_\odot$), SN 1980K at year 30 (0.12–0.30 $M_\odot$) and Cas A at year 330 (∼1.1 $M_\odot$) are broadly consistent with these trends. These dust masses suggest that dust formation in Type IIb SN ejecta such as SN 1993J and Cas A is just as effective as in Type II SN ejecta such as those of SN 1987A and SN 1980K. Our dust mass estimate for Cas A is in broad agreement with the dust mass of 0.4–0.7 $M_\odot$ recently derived from a spatially resolved analysis of *Spitzer* and *Herschel* IR and submillimetre imaging data for Cas A (De Looze et al. 2016). Reasonably good multi-epoch data exist for a number of other SNe and SNRs, including SN1993J and SN1979C, which will provide an excellent opportunity to probe further the evolution of dust formation in these objects.

ACKNOWLEDGEMENTS

AB's work was supported by a UK STFC Research Studentship (ST/K502406/1). MJB acknowledges support from STFC grant ST/M001334/1 and, since 2016 June 1, from European Research Council (ERC) Advanced Grant SNDUST 694520.

REFERENCES

Arendt R. G., Dwek E., Moseley S. H., 1999, ApJ, 521, 234
Arendt R. G., Dwek E., Kober G., Rho J., Hwang U., 2014, ApJ, 786, 55
Barbon R., Ciatti F., Rosino L., 1982, A&A, 116, 35
Barlow M. J. et al., 2010, A&A, 518, L138
Baron E., Hauschildt P. H., Branch D., Wagner R. M., Austin S. J., Filippenko A. V., Matheson T., 1993, ApJ, 416, L21
Bevan A., Barlow M. J., 2016, MNRAS, 456, 1269
Biscaro C., Cherchneff I., 2014, A&A, 564, A25
Buta R. J., 1982, PASP, 94, 578
Chevalier R. A., 1986, ApJ, 308, 225
Chevalier R. A., Fransson C., 1992, ApJ, 395, 540
Chevalier R. A., Fransson C., 1994, ApJ, 420, 268
Chugai N. N., Danziger I. J., 1994, MNRAS, 268, 173
De Looze I., Barlow M. J., Swinyard B. M., Rho J., Gomez H. L., Matsuura M., Wesson R., 2016, MNRAS, in press
DeLaney T. et al., 2010, ApJ, 725, 2038
Draine B. T., Lee H. M., 1984, ApJ, 285, 89
Dunne L., Eales S., Ivison R., Morgan H., Edmunds M., 2003, Nature, 424, 285
Dunne L. et al., 2009, MNRAS, 394, 1307
Dwek E. et al., 1983, ApJ, 274, 168
Dwek E., Galliano F., Jones A. P., 2007, ApJ, 662, 927
Fesen R. A., Becker R. H., 1988, BAAS, 20, 962
Fesen R. A., Becker R. H., 1990, ApJ, 351, 437
Fesen R. A., Matonick D. M., 1994, ApJ, 428, 157
Fesen R. A., Hurford A. P., Matonick D. M., 1995, AJ, 109, 2608
Fesen R. A. et al., 1999, AJ, 117, 725
Fesen R. A., Morse J. A., Chevalier R. A., Borkowski K. J., Gerardy C. L., Lawrence S. S., van den Bergh S., 2001, AJ, 122, 2644
Fesen R. A. et al., 2006, ApJ, 645, 283
Filippenko A. V., Matheson T., Ho L. C., 1993, ApJ, 415, L103
Fox O. D. et al., 2014, ApJ, 790, 17
Fransson C. et al., 2005, ApJ, 622, 991
Freedman W. L. et al., 1994, ApJ, 427, 628
Gall C., Hjorth J., Andersen A. C., 2011, A&AR, 19, 43
Gall C. et al., 2014, Nature, 511, 326
Garnavich P. M., Ann H. B., 1993, BAAS, 182, 8302
Gomez H. L. et al., 2012, ApJ, 760, 96
Gotthelf E. V., Koralesky B., Rudnick L., Jones T. W., Hwang U., Petre R., 2001, ApJ, 552, L39
Indebetouw R. et al., 2014, ApJ, 782, L2
Karachentsev I. D., Sharina M. E., Huchtmeier W. K., 2000, A&A, 362, 544
Kozma C., Fransson C., 1998, ApJ, 496, 946
Krause O., Birkmann S. M., Rieke G. H., Lemke D., Klaas U., Hines D. C., Gordon K. D., 2004, Nature, 432, 596
Krause O., Birkmann S. M., Usuda T., Hattori T., Goto M., Rieke G. H., Misselt K. A., 2008, Science, 320, 1195
Lucy L., Danziger I., Gouiffes C., Bouchet P., 1989, in Tenorio-Tagle G., Moles M., Melnick J., eds, Proc. IAU Colloq. 120, Structure and Dynamics of the Interstellar Medium, Lecture Notes in Physics, Vol. 350. Springer-Verlag, Berlin, p. 164
Matheson T. et al., 2000a, AJ, 120, 1487
Matheson T., Filippenko A. V., Ho L. C., Barth A. J., Leonard D. C., 2000b, AJ, 120, 1499
Matsuura M. et al., 2015, ApJ, 800, 50
Maund J. R., Smartt S. J., Kudritzki R. P., Podsiadlowski P., Gilmore G. F., 2004, Nature, 427, 129
Milisavljevic D., Fesen R. A., 2013, ApJ, 772, 134
Milisavljevic D., Fesen R. A., Chevalier R. A., Kirshner R. P., Challis P., Turatto M., 2012, ApJ, 751, 25
Montes M. J., Van Dyk S. D., Weiler K. W., Sramek R. A., Panagia N., 1998, ApJ, 506, 874
Morgan H. L., Edmunds M. G., 2003, MNRAS, 343, 427
Nozawa T., Kozasa T., Tominaga N., Maeda K., Umeda H., Nomoto K., Krause O., 2010, ApJ, 713, 356
Reed J. E., Hester J. J., Fabian A. C., Winkler P. F., 1995, ApJ, 440, 706
Rest A. et al., 2011, ApJ, 732, 3
Rho J. et al., 2008, ApJ, 673, 271
Ripero J. et al., 1993, IAU Circ., 5731, 1
Sibthorpe B. et al., 2010, ApJ, 719, 1553
Smith N., Foley R. J., Filippenko A. V., 2008, ApJ, 680, 568
Smith N., Silverman J. M., Filippenko A. V., Cooper M. C., Matheson T., Bian F., Weiner B. J., Comerford J. M., 2012, AJ, 17, 6
Storey P. J., Zeippen C. J., 2000, MNRAS, 312, 813
Stritzinger M. et al., 2012, ApJ, 756, 173
Sugerman B. E. K. et al., 2006, Science, 313, 196
Sugerman B. E. K. et al., 2012, ApJ, 749, 170
Tran H. D., Filippenko A. V., Schmidt G. D., Bjorkman K. S., Jannuzi B. T., Smith P. S., 1997, PASP, 109, 489
Wesson R., Barlow M. J., Matsuura M., Ercolano B., 2015, MNRAS, 446, 2089
Wheeler J. C., Filippenko A. V., 1996, in Kuhn T. S., ed., Proc. IAU Colloq. 145, Supernovae and Supernova Remnants. Cambridge Univ. Press, Cambridge, p. 241
Wooden D. H., Rank D. M., Bregman J. D., Witteborn F. C., Tielens A. G. G. M., Cohen M., Pinto P. A., Axelrod T. S., 1993, ApJS, 88, 477
Zeippen C. J., 1987, A&A, 173, 410
Zhang T., Wang X., Zhou X., Li W., Ma J., Jiang Z., Li Z., 2004, AJ, 128, 1857

This paper has been typeset from a TEX/LATEX file prepared by the author.